

Phase transition characteristics of Faraday waves*

Peizhao Li,¹ Tiancheng Yu,¹ Xuechang Tu,² Han Yan,¹ Wei Wang,¹ and Luqun Zhou^{1,†}

¹*School of Physics, Peking University, Beijing*

²*School of Electronics Engineering and Computer Science, Peking University, Beijing*

(Dated: May 16, 2023)

Through experimentation, we have discovered that under varying driving conditions, the Faraday waves undergo two abrupt transitions in spatiotemporal order: onset and instability. The driving amplitudes and frequencies corresponding to these two transitions follow power-law relationships. The exponent of the power-law for the onset can be used to categorize different liquids into two distinct classes, which primarily reflects the differential contribution of surface tension and viscous forces in the surface wave dispersion relation. Furthermore, the exponent of the power-law for the instability serves as a quantitative indicator of the non-Newtonian properties of the liquid. Based on our experimental findings, we develop a phenomenological theoretical model that provides a comprehensive understanding of the properties of the Faraday pattern.

INTRODUCTION

The phenomenon of regular pattern formation on the surface of a fluid subjected to periodic vertical external forces, known as the Faraday pattern, was first discovered by M. Faraday in 1831 [1]. Over the past few centuries, a multitude of experimental results have been reported, including pattern selection [2–8], bifurcation [9], oscillon [10–12], lattice defects [13], and turbulence [14–18]. These extensive investigations have greatly enriched our understanding of the Faraday waves and even nonlinear systems.

For a system undergoing a transition from order to disorder, undoubtedly, the transition parameters that correspond to its phase transition point and the behavior of the system in the vicinity of the phase transition point are the two fundamental issues that merit our attention. The pertinent research was initially conducted by Tuffillaro et al. in 1989 [14], where they considered the spatial auto-correlation function of Faraday waves and obtained the phase transition curve. Subsequent studies have further augmented and refined the system's phase diagram on the one hand [5], and explored the mechanism of the phase transition using different methods on the other hand [16, 18]. These studies have furnished us with a comprehensive and lucid portrayal of the Faraday wave phase transition.

In this article, we approach the Faraday pattern transitions from a different perspective, focusing on the relationship between the external driving amplitudes and frequencies. Through experiments, we discover power-law relationships between the transition driving acceleration and frequency at the onset of the Faraday waves. Based on this power-law exponent, we define a characteristic wave number of the fluid surface wave to characterize its dynamical properties. Furthermore, we find that with a further increase in the driving amplitude, the Faraday waves also undergo a stable-to-unstable transition, and the transition acceleration and frequency also follow a power-law relationship, which may reflect the non-

Newtonian nature of the fluid. Based on experimental data, we develop a phenomenological theoretical model that provides a unified understanding of the Faraday pattern properties.

METHODS

The experimental setup employed in this study is illustrated in FIG. 1, which consists of a cylindrical container with a diameter of 14 cm, filled with a liquid sample that is 2 cm thick.

The excitation signal generated by the signal generator is amplified by the power amplifier to drive the modal exciter (Sinocera Piezotronics, JZK-100), causing the liquid sample to vibrate sinusoidally at different amplitudes and frequencies. Meanwhile, the oscilloscope displays the accelerometer signal amplified by the charge amplifier in real-time.

To capture the shape of the liquid surface Faraday waves, we employ a high-speed camera (AOS Technologies AG, S-PRI F2) to record the reflection of light on the liquid surface, which is further enhanced with the addition of a drop of ink to increase the image contrast. The entire experimental setup is maintained at a constant temperature of 26°C.

The behaviors of the Faraday waves exhibit distinct phase transitions: at low driving amplitudes, the liquid moves uniformly with the container, and the surface displays no observable pattern (FIG. 2a). Beyond a threshold A_{c1} , the surface exhibits the spontaneous emergence of isolated oscillators, which gradually stabilize in amplitude (FIG. 2b). Increasing the driving amplitude further causes the oscillators to persist independently until reaching another threshold A_{c2} , beyond which they collide and merge, resulting in a disordered surface pattern (FIG. 2c). We term the transition from no pattern to pattern as the "onset," and the transition from ordered to disordered as "instability" for clarity.

We can easily determine the transition point at which

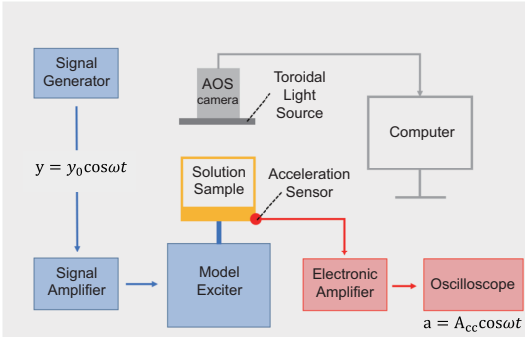


FIG. 1. Diagram of the experimental setup

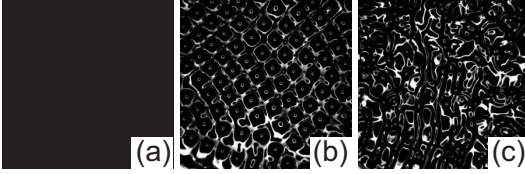


FIG. 2. Surface patterns of 5g/L xanthan gum fluid under different driving conditions: (a) no Faraday waves ($f = 60\text{Hz}$, $A_{cc} = 3.92\text{g}$); (b) ordered Faraday waves ($f = 60\text{Hz}$, $A_{cc} = 5.77\text{g}$); (c) disordered Faraday waves ($f = 60\text{Hz}$, $A_{cc} = 7.00\text{g}$).

the onset of Faraday waves occurs by visual inspection, while for the transition point at which the Faraday waves become unstable, we use two methods to measure the degree of order in both temporal and spatial dimensions of the data obtained from the experiments.

In the temporal dimension, we select a frame as the starting point from the time sequence images obtained from the experiments and calculate the autocorrelation function between subsequent frames and the starting point:

$$r(t) = \frac{\sum_{i,j} (P_{ij}(t) - \bar{P}(t))(P_{ij}(0) - \bar{P}(0))}{\sqrt{\sum_{i,j} (P_{ij}(t) - \bar{P}(t))^2 (P_{ij}(0) - \bar{P}(0))^2}} \quad (1)$$

where P_{ij} represents the gray value of the (i, j) pixel in the image. Furthermore, for the case where the driving period is T and the acceleration amplitude is A_{cc} , we calculate the reproducibility:

$$F(T, A_{cc}) = \frac{r(T) + r(2T) + r(3T)}{3} \quad (2)$$

Since the probability of two frames being accidentally correlated in the time sequence images is very low (about 10^{-7}), the reproducibility can well reflect the temporal periodicity of the system.

In the spatial dimension, we employ a clustering algorithm (FIG. 3) to categorize images of the liquid surface into ordered and disordered classes in the spatial dimension, using the confidence probability p of each image's classification as a measure of its orderliness. To

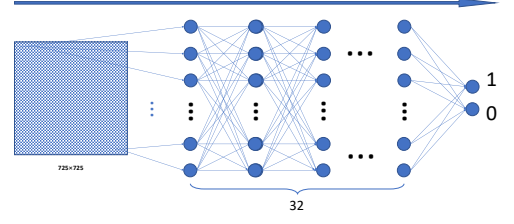


FIG. 3. Schematic diagram of clustering algorithm

ensure a representative image set and reduce extraneous factors, we exclude the top 15% and bottom 30% of images with the highest and lowest orderliness, respectively, and calculate the average degree of order for the remaining images as the spatial orderliness q . The algorithm uses distribution features to classify the images, and if a small change in parameters results in most images switching classes, we conclude that the Faraday wave's spatial characteristics have changed.

RESULTS

Our experiments reveal two phase transitions in the Faraday pattern: the onset and instability transitions. We observe a significant power-law relationship between the driving amplitude and frequency of both transitions, with corresponding exponents summarized in TABLE I. Xanthan gum at different concentrations exhibit onset transition exponents around $3/2$, while silicone oil and various glycerol concentrations display transition exponents of approximately $5/3$, consistent with previous studies on CO_2 liquid-gas interface[19] and paraffin oil[13] (TABLE I). For Newtonian fluids, the instability transition exponent remains constant and close to $5/3$ regardless of viscosity. Conversely, for the same non-Newtonian fluid, the transition exponent decreases linearly with increasing viscosity. We will provide a detailed analysis of our experimental findings in subsequent sections.

Phase transition characteristics of Faraday waves

We observe the surface patterns of different liquids under various driving conditions. To locate the transition point at which the Faraday waves become unstable, we take a 5 g/L solution of xanthan gum as an example and plot the temporal variation of the two indicators r and p under different driving conditions with a frequency of $f = 25\text{Hz}$ in FIG. 4.

At low driving amplitudes (FIG. 4a), r varies periodically with time at a frequency identical to that of the driving force, while p remains close to 1 in most cases and only periodically exhibits low values at a frequency that

Liquid Type	Liquid	viscosity/Pa-s	Onset Transition Exponent	Instability Transition Exponent
Newtonian fluids	CO ₂ liquid-gas interface[19]		1.76	
	Paraffin oil[13]	0.05	1.70	
	Silicone oil	0.35	1.67 ± 0.03	1.75 ± 0.04
	Glycerin	1.2	1.75 ± 0.03	1.64 ± 0.02
	85%Glycerin	0.13	1.67 ± 0.03	1.64 ± 0.01
	50%Glycerin	0.05	1.75 ± 0.03	1.59 ± 0.03
Non-Newtonian fluids	2.5g/L Xanthan gum solution	20	1.52 ± 0.03	1.78 ± 0.02
	5g/L Xanthan gum solution	30	1.48 ± 0.02	1.51 ± 0.02
	10g/L Xanthan gum solution	70	1.49 ± 0.02	1.34 ± 0.01
	15g/L Xanthan gum solution	80	1.49 ± 0.01	1.24 ± 0.03

TABLE I. Summary table of onset and instability transition indices for fluid Faraday waves.

is twice the driving force frequency. This is because, for a solitary wave in an ordered state, the shape of the liquid surface is mainly determined by the disordered noise when it vibrates to the equilibrium position. As the driving amplitude increases (FIG. 4b), r rapidly drops from 1 to near 0, and p remains mostly low, only occasionally exhibiting high values when the liquid surface forms more ordered structures.

To further analyze the behavior of the 5g/L xanthan gum solution, we calculated the time reproducibility F and space orderliness q based on the r and p values obtained under different driving conditions. The variations of F and q with the driving amplitude A_{cc} under a driving frequency of $f = 25\text{Hz}$ are shown in FIG. 5. As the driving amplitude increases, both F and q initially remain close to 1, but once a transition value is reached, they suddenly drop to nearly 0, corresponding to a phase transition from order to disorder in both time and space. As can be seen from the FIG. 5, the transition position where the time reproducibility represented by F and the spatial orderliness represented by p undergo a phase transition is within the range of the measurement sampling interval. Due to the essentially coincident time-space phase transition point, we no longer differentiate between the two, and instead use the value of A_{c2} , corresponding to when F drops to 0.5, as the instability phase transition point of the pattern.

The power-law relationship between the transition amplitudes and frequencies

By utilizing the method described in the previous section, we are able to experimentally determine the onset transition amplitude A_{c1} and the instability transition amplitude A_{c2} under a fixed driving frequency f . Taking 5g/L of xanthan gum as an example, we plot the A_{c1} and A_{c2} at different f together to construct the phase diagram of the system, as illustrated in the inset of FIG. 6. The phase diagram divides the driving parameter space into three regions: region I where no pattern is formed,

region II where stable patterns emerge, and region III where unstable patterns arise.

Furthermore, we apply a double logarithmic scale to fit the relationship between A_c and f and a strong power-law correlation between the two. The power-law exponents for A_{c1} and A_{c2} are determined to be 1.48 and 1.51, respectively. This finding raises an important question: if $A_c \propto f$ or $A_c \propto f^2$ at the transition point, it implies that the transition phenomenon is affected by the driving speed or amplitude from the external environment. However, our experimental data clearly indicates that $A_c \propto f^{1.5}$, indicating that this transition exponent is determined by intrinsic properties of the system's dynamics. In subsequent sections, we analyze these two transition exponents independently.

The onset transition exponent

We first focus on the transition amplitude A_{c1} for the onset of oscillations. To investigate this further, we conduct the same experiment using various concentrations of xanthan gum, glycerol-water mixtures, and silicone oil. We plot the double-logarithmic fitting curves for A_{c1} versus f and compile their slopes in TABLE I. Despite the different transition amplitudes required for the onset of oscillations at the same driving frequency for each liquid, the power-law relationship between A_{c1} and f remains consistent and the power-law exponents exhibit distinct distribution characteristics. Specifically, different concentrations of xanthan gum exhibit power-law exponents around 3/2, whereas silicone oil and different concentrations of glycerol exhibit power-law exponents around 5/3.

We further analyze this result theoretically:

Based on the findings by S. Fauve et al. in 1992 [19], in the absence of air density and viscosity, a transition amplitude a_{c1} for the Faraday pattern to appear is related to the driving frequency f by:

$$A_{c1} \approx 8\pi f k \frac{\nu}{\rho} \quad (3)$$

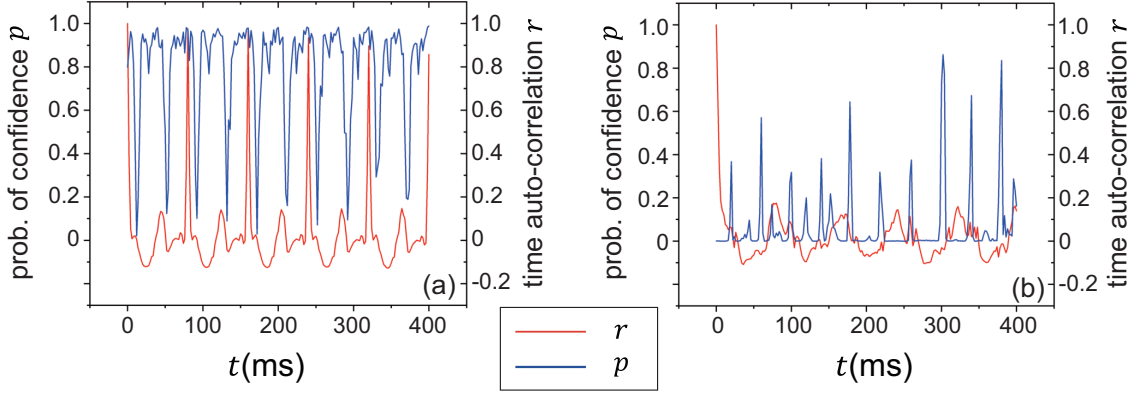


FIG. 4. The figure above shows the plots of the time autocorrelation function r (in red) and spatially ordered confidence probability p (in blue) of 5g/L xanthan gum solution under different driving conditions. (a) $f = 25\text{Hz}$, $A_{cc} = 1.83\text{g}$; (b) $f = 25\text{Hz}$, $A_{cc} = 2.34\text{g}$.

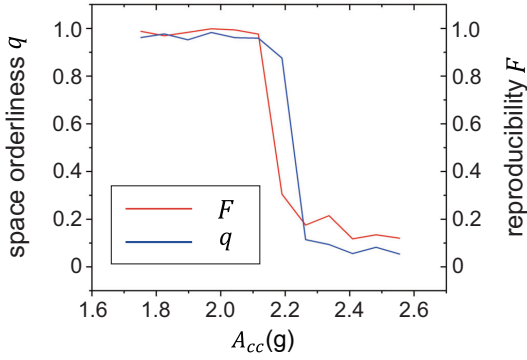


FIG. 5. Graph of the variation of the time reproducibility F and spatial order degree q of 5g/L xanthan gum solution with respect to the amplitude A_{cc} at a driving frequency of 25Hz.

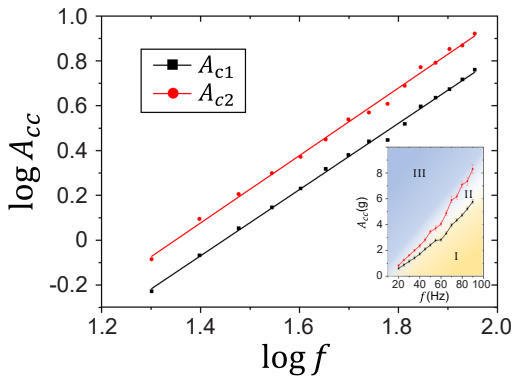


FIG. 6. $\log A$ - $\log f$ linear fitting graph of 5g/L xanthan gum fluid. Transition onset amplitude $A_{c1} \propto f^{1.48}$, corresponding to $r = 0.9987$; instability amplitude $A_{c2} \propto f^{1.51}$, corresponding to $r = 0.9983$. (Insert FIG.) Faraday waves phase diagram. Region I: No pattern; Region II: Stable pattern; Region III: Unstable pattern.

where k is the wave vector of the liquid surface waves and ν is the dynamic viscosity of the liquid. For viscous fluids, the surface shallow water waves satisfy the dispersion relation [3]:

$$\omega^2 = [gk + \frac{\alpha}{\rho}k^3 + 4(\frac{\nu}{\rho})^2k^4] \tanh(Hk) \quad (4)$$

Here, g is the acceleration due to gravity, α is the liquid surface tension coefficient, ρ is the liquid density, and H is the liquid depth. In our experiment, $k \sim 400 - 1000\text{m}^{-1}$, $Hk \gg 1$, and $\tanh(Hk) \approx 1$, while $gk \ll \frac{\alpha}{\rho}k^3$, $(\frac{\nu}{\rho})^2k^4$. Thus, the dispersion is mainly determined by the cubic and quartic terms of k , and the ratio of the two terms is:

$$\eta = \frac{w_{k^4}^2}{w_{k^3}^2} = \frac{4\nu^2k}{\rho\alpha} \quad (5)$$

For different concentrations of xanthan gum solution ($\nu \sim 10\text{Pa}\cdot\text{s}$, $\rho \sim 10^3\text{kg/m}^3$, $\alpha \sim 10^{-2}\text{N/m}$), $\eta \sim 10^4$, the dispersion relation is mainly determined by the quartic term k^4 , resulting in $k \propto \omega^{1/2}$ and $a_{c1} \propto f^{3/2}$, which is consistent with our experimental observations. Similarly, for silicon oil and glycerol-water solutions ($\nu \sim 10^{-2}\text{Pa}\cdot\text{s}$, $\rho \sim 10^3\text{kg/m}^3$, $\alpha \sim 10^{-2}\text{N/m}$), $\eta \sim 10^{-2}$ the dispersion relation is mainly determined by the cubic term k^3 , leading to $k \propto f^{2/3}$ and $a_{c1} \propto f^{5/3}$. These theoretical results are in good agreement with our experimental observations.

We can extract a characteristic wave number k_c from Eq. (5) to characterize the dynamic properties of the Faraday pattern:

$$k_c = \frac{\rho\alpha}{4\nu^2} \quad (6)$$

The relationship between a_{c1} and f depends on the relative magnitude of k_c and k : when $k_c \ll k$, $a_{c1} \propto f^{3/2}$; when $k_c \gg k$, $a_{c1} \propto f^{5/3}$.

The instability transition exponent

Next, we analyze the transition amplitude for instability, A_{c2} . As shown in TABLE I, the transition exponent for instability remains nearly constant and close to 5/3 for Newtonian fluids, irrespective of their viscosity. Conversely, for non-Newtonian fluids, the transition exponent decreases linearly with increasing viscosity.

We provide a semi-quantitative explanation of this result:

Starting from the Navier-Stokes equations for an ideal fluid incorporating surface tension, we find the gradient for it and obtain the generalized equations by adding the viscous term and generalizing the acceleration term:

$$\frac{\partial v}{\partial t} = g^* + \frac{\alpha}{\rho} \nabla \left(\frac{\partial^2 \zeta}{\partial x^2} + \frac{\partial^2 \zeta}{\partial y^2} \right) + \frac{\nu}{\rho} \Delta v \quad (7)$$

where g^* representing the effective gravitational acceleration in the platform's reference frame. For the case involved in this experiment, we can write:

$$g^* = g + A_{cc} \cos(2\pi ft + \phi) \quad (8)$$

where g and A_{cc} are constant vectors.

We calculate the scalar product of v on both sides of Eq. (7) and average it over the spatial region of oscillation. By applying the scattering theorem (which states that the scattering of the velocity field of an incompressible fluid is zero), the spatial integral of the second term on the right side of Eq. (7) can be reduced to an integral with zero results at the region boundary. We can handle the last term using the divisional integration approach:

$$\frac{1}{2} \frac{\partial \langle |v|^2 \rangle}{\partial t} = \langle v g^* \rangle - \frac{\nu}{\rho} \langle \nabla v : \nabla v \rangle \quad (9)$$

where $\nabla v : \nabla v = (\partial_k v_i)(\partial_k v_i)$.

As the system is subjected to steady periodic vibrations, the time derivative of the spatial average in the left-hand side equation is zero. The subscript m is used to denote the amplitude of each vibrational quantity, and hence the following approximate expression can be obtained:

$$v_m A_{cc} \propto \frac{\nu}{\rho} k^2 v_m^2 \quad (10)$$

where k is the wave number of surface tension gravity waves. From the energy point of view, this equation can be approximated as the energy balance equation, i.e. the work done by the external "gravitational field" is balanced by the energy dissipated by the viscous dissipation of the oscillating fluid.

If we denote the amplitude of the oscillator as A_m , then we have $v_m \sim A_m f$. Substituting this expression into Eq. (10), we obtain:

$$A_{cc} \sim \frac{\nu}{\rho} k^2 f A_m \quad (11)$$

The instability of Faraday waves is attributed to the interaction between neighboring oscillators, which occurs when the diameter of a single oscillator exceeds the wavelength λ . This interaction causes the originally independent oscillators to become coupled and leads to instability. Moreover, the shape of the oscillators is nearly constant, which means $d \propto A_m$. When the pattern becomes unstable, $A_m \sim 1/k$, that is:

$$A_{c2} \sim \frac{\nu}{\rho} k f \quad (12)$$

This transition driving amplitude A_{c2} corresponds to the Faraday wave pattern and has a similar form to Eq. (3).

For the Newtonian fluid used in the experiment with relatively low viscosity, its viscosity remains constant, and the wavenumber is proportional to $f^{2/3}$. Substituting this into Eq. (12), we obtain

$$A_{c2} \propto f^{5/3} \quad (13)$$

For non-Newtonian fluids, the relationship between viscosity and oscillation frequency follows[20]:

$$\nu = \nu_0 f^{n-1} \quad (14)$$

where $n < 1$ and decreases with increasing ν_0 , indicating a more significant shear-thinning effect in fluids with higher initial viscosity. In the experiment, the xanthan gum solution experiences a drop in viscosity to $10^{-2} \text{Pa}\cdot\text{s}$ due to the shear-thinning effect when it becomes unstable. Therefore, its dispersion relation can be approximated as $k \propto f^{2/3}$. Substituting this into Eq. (12) gives:

$$A_{c2} \propto f^{n+2/3} \quad (15)$$

The power-law exponent n and ν_0 for the xanthan gum solution can be related through a fitted curve obtained from the experimental data, given by $n = 1.07 - 0.0075\nu_0$. This suggests that the shear-thinning behavior is absent when the viscosity is zero, as $n \approx 1$. As the viscosity increases, the shear-thinning effect becomes more prominent, which agrees with the experimental findings.

It should be noted that in the preceding section, the shear-thinning effect was not taken into account when determining the driving amplitude for the onset of oscillations. This is because, prior to the onset of oscillations, there is no shear rate at the liquid surface and the liquid's dynamic properties are governed only by its intrinsic viscosity ν_0 . However, the shear rate at the liquid surface is significant before and after the instability, making the shear-thinning effect important and cannot be neglected.

CONCLUSION

In this study, we have conducted experiments to investigate the temporal reproducibility and spatial orderliness of Faraday waves in different liquids under various

driving conditions. We have discovered a discontinuous change in the degree of spatial orderliness and temporal reproducibility of the waves at the onset of instability, and we have found that the transition driving amplitude and frequency at this point follow a power-law relationship. The transition exponents for the onset of wave patterns have been found to be $3/2$ and $5/3$ for two groups of liquids, respectively, which depend on the relative importance of the surface tension and viscosity terms in the shallow-water wave dispersion relation. We have also proposed a characteristic wave number, k_c , that characterizes the dynamical properties of Faraday waves.

Regarding the instability of Faraday waves, we have observed that the transition exponents of Newtonian fluids are near $5/3$, while those of non-Newtonian fluids decrease almost linearly with increasing viscosity. We have hypothesized that the instability of the pattern originates from the interaction between neighboring oscillators after the increase in their size. Through a semi-quantitative analysis, we have provided a theoretical explanation for the transition exponent of Newtonian fluids and proposed that the shear-thinning effect may cause the transition exponent of non-Newtonian fluids to vary with viscosity.

Restricted by experimental conditions, our study is limited to the cases of $\eta \gg 1$ and $\eta \ll 1$, where η is the dimensionless viscosity, and further experiments are needed to verify the findings for the case of $\eta \sim 1$, where the contribution of the surface tension and viscosity terms to the shallow-water wave dispersion relation is of similar magnitude. Additionally, the understanding of the instability of non-Newtonian fluids requires further theoretical exploration.

The work is supported by the Undergraduate Teaching Reform Project at Peking University(JG2023003). We appreciate Prof. Qi Ouyang for many useful discussions.

* Peizhao Li and Tiancheng Yu contributed equally to this work

† email: zhoulq@pku.edu.cn

- [1] M. Faraday, *Philosophical Transactions of the Royal Society of London* **121**, 299 (1831), publisher: Royal Society.
- [2] T. B. Benjamin, F. J. Ursell, and G. I. Taylor, *Proceedings of the Royal Society of London. Series A. Mathematical and Physical Sciences* **225**, 505 (1954), publisher: Royal Society.
- [3] W. Zhang and J. Viñals, *Journal of Fluid Mechanics* **336**, 301 (1997), publisher: Cambridge University Press.
- [4] D. Binks and W. van de Water, *Physical Review Letters* **78**, 4043 (1997), publisher: American Physical Society.
- [5] C. Wagner, H. W. Müller, and K. Knorr, *Physical Review Letters* **83**, 308 (1999).
- [6] P. Chen and J. Viñals, *Physical Review E* **60**, 559 (1999), publisher: American Physical Society.
- [7] N. Périnet, D. Juric, and L. S. Tuckerman, *Journal of Fluid Mechanics* **635**, 1 (2009), publisher: Cambridge University Press.
- [8] A. C. Skeldon and A. M. Rucklidge, *Journal of Fluid Mechanics* **777**, 604 (2015), publisher: Cambridge University Press.
- [9] S. Douady, *Journal of Fluid Mechanics* **221**, 383 (1990), publisher: Cambridge University Press.
- [10] H. Arbell and J. Fineberg, *Physical Review Letters* **85**, 756 (2000).
- [11] H. Xia, T. Maimbourg, H. Punzmann, and M. Shats, *Physical Review Letters* **109**, 114502 (2012).
- [12] H.-Y. Chen, C.-Y. Liu, and L. I, *Physical Review Fluids* **3**, 064401 (2018).
- [13] A. B. Ezersky, D. A. Ermoshin, and S. V. Kiyashko, *Physical Review E* **51**, 4411 (1995).
- [14] N. B. Tuffillaro, R. Ramshankar, and J. P. Gollub, *Physical Review Letters* **62**, 422 (1989).
- [15] W. B. Wright, R. Budakian, and S. J. Putterman, *Physical Review Letters* **76**, 4528 (1996).
- [16] I. Shani, G. Cohen, and J. Fineberg, *Physical Review Letters* **104**, 184507 (2010).
- [17] A. von Kameke, F. Huhn, G. Fernández-García, A. P. Muñozuri, and V. Pérez-Muñozuri, *Physical Review Letters* **107**, 074502 (2011).
- [18] N. Francois, H. Xia, H. Punzmann, S. Ramsden, and M. Shats, *Physical Review X* **4**, 021021 (2014).
- [19] S. Fauve, K. Kumar, C. Laroche, D. Beysens, and Y. Garrabos, *Phys. Rev. Lett.* **68**, 3160 (1992), publisher: American Physical Society.
- [20] M. M. Cross, *Rheologica Acta* **18**, 609 (1979).